

Localizing excitations in a quantum computer with perpetually coupled qubits

L.F. Santos¹, M.I. Dykman¹, and M. Shapiro²

¹*Department of Physics and Astronomy, and ²Department of Mathematics,
Michigan State University, East Lansing, MI 48824*

F.M. Izrailev

Instituto de Física, Universidad Autónoma de Puebla, Puebla 72570, México

(Dated: May 23, 2019)

Strong many-particle localization is studied in a 1D system of interacting fermions and an equivalent system of coupled qubits. We propose a sequence of on-site fermion energies, or qubit transition frequencies, that eliminates resonant excitation transfer between both nearest and remote neighbors. It leads to quasi-exponential decay of the single-particle transition amplitude, which can be analytically described. It also leads to a large lifetime of strongly localized many-particle states, that exceeds the reciprocal hopping frequency by six orders of magnitude for a comparatively narrow bandwidth of on-site energies. The proposed energy sequence is robust with respect to small errors. This makes quantum computing with time-independent qubit coupling viable.

PACS numbers: 03.67.Lx,72.15.Rn,75.10.Pq,73.23.-b

I. INTRODUCTION

In many proposed physical implementations of a quantum computer (QC) the qubit-qubit interaction is not turned off [1, 2, 3, 4, 5, 6, 7]. The interaction may lead to excitation hopping from one qubit to another. However, control and measurement in quantum computing should be presumably performed in the basis of states localized on individual qubits. Therefore it is essential that, between operations, excitations remain localized. This makes the problem of localization central for quantum computing with perpetually coupled qubits.

In a multi-excitation system like a QC, hopping is a many-body effect, it can be accompanied by the change of state of several excitations. Many-particle hopping and localization are phenomena of a fairly general interest. They have been attracting attention in different areas of physics, in particular in condensed matter physics in the context of metal-insulator transition in interacting electron systems [8]. The problem of many-particle localization is intractable with a classical computer, because the Hilbert space is exponentially large. QC's with perpetually coupled qubits provide a unique means for investigating it in controllable setting.

In this paper we study strong localization, where each excitation is mainly confined to one qubit (one site). A well-known argument suggests that it is hard to strongly localize a many-particle system when the on-site energies are random and uniformly distributed within a finite-width band [9]. Indeed, consider a state where particles occupy N sites. For short-range hopping it is directly coupled to $\propto N$ other N -particle states. With probability $\propto N$ one of them will be in resonance with the initial state. For large N this leads to state hybridization in such a disordered system, which occurs over time $\sim J^{-1}$, where J is the intersite hopping integral (we set $\hbar = 1$).

In a QC, the quantity J is determined by the qubit-qubit interaction and usually characterizes the rate of

two-qubit operations. At the same time, the qubit energies are not random and often can be individually controlled [2].

Elegant approaches to quantum computation with perpetually interacting qubits were discussed recently [10, 11]. However, an implementation of the algorithm by Zhou *et al.* [10] requires that the interaction be turned off at the initiation stage. On the other hand, the approach of Benjamin and Bose [11] requires an extremely broad bandwidth of qubit energies. Localization and quantum chaos for a system with an energy bandwidth proportional to the number of qubits was studied by Berman *et al.* [12].

The localization problem has two sides. One is the traditional problem of localization of stationary states of a many-particle system. The other is the problem of the time it takes for a localized many-particle state to hybridize with a nearly resonant state, which we will call the localization lifetime t_{loc} . In a QC all states have a finite coherence time due to coupling to the environment and external noise. For QC operation it will suffice if delocalization does not occur during this time. For most of the proposed models of a QC, the coherence time is $\lesssim 10^5 - 10^6 J^{-1}$. Therefore it is sufficient to have the localization lifetime $\gtrsim 10^5 - 10^6 J^{-1}$. Such lifetime-based formulation of the many-particle localization problem is relevant to condensed-matter systems, too, because of finite decay and decoherence times of quasiparticles for nonzero temperatures.

Here we construct a bounded sequence of on-site energies in a 1D chain and show that it leads to a long localization lifetime. We provide evidence that it also leads to strong localization of many-particle stationary states in sections of the chain with length up to 12 sites. This approach is in a sense a construction of an efficiently localizing on-site disorder.

In a QC, a sequence of on-site energies can be constructed simply by tuning the energies of individual

qubits. Because the tuning range is usually limited, it is important to keep the energy bandwidth small. A smaller width leads also to a higher speed of quantum gate operations, particularly if they involve changing qubit energies [13].

To strongly localize one particle, the difference between excitation energies on neighboring sites should be much larger than J . However, this is not sufficient even for nearest neighbor coupling. The energies of remote sites should also differ. The further away the sites are, the smaller their energy difference may be. For our energy sequence, the single-particle transition amplitude displays nearly exponential decay with distance. We find rigorous bounds on the decay exponent.

For many-particle localization one has to suppress not only single-particle, but also combined resonances, where several interacting excitations make a transition simultaneously. This is a hard problem. However, with the increasing “order” of the transition, i.e., the number of involved excitations and/or intermediate virtual states, the effective hopping integral may quickly fall off, leading to increasing transition time. Then to obtain a desired lifetime of a localized state it is sufficient to eliminate resonances up to a certain order. We explicitly show how to do it up to at least fifth order, for our sequence.

In a realistic system, it will be possible to tune qubit energies only with certain precision. We study the effect of errors in the energies on localization and show that our sequence is stable with respect to small errors. We also demonstrate that, in terms of strong localization, the constructed energy sequence is by far superior to fully random on-site energies with the same overall bandwidth.

The paper is organized as follows. In Sec. II we discuss the Hamiltonian of coupled qubits and introduce a physically motivated one-parameter sequence of on-site energies. In Sec. III one-particle localization is discussed and quasi-exponential decay of the transition amplitude is demonstrated. A rigorous proof of such decay is provided in the Appendix. In Sec. IV the inverse participation ratio is calculated for many-particle excitations in a section of a 1D chain. It can be made very close to one in a broad range of the parameter of the on-site energy sequence, but also displays sharp resonant peaks as a function of this parameter. The lifetime of localized states is discussed in Sec. V. A modification of the energy sequence allows one to open a gap in the spectrum of combined many-excitation transitions up to 5th order, which is sufficient for a long localization lifetime. The role of errors in the on-site energies is studied, and robustness of the results with respect to these errors is demonstrated. In Sec. VI a highly symmetric period-doubling sequence of on-site energies is studied along with a sequence of uncorrelated on-site energies. Both are by far inferior, in terms of localization, to the sequence discussed in Secs. II-V. Sec. VII contains concluding remarks.

II. THE MODEL OF INTERACTING QUBITS

In this paper we do not discuss gate operations. We assume that the parameters of the system, including qubit excitation energies, are independent of time, and no time-dependent fields, like microwave radiation, are modulating the system. We also do not discuss decay and decoherence. The goal is to study localization of excitations between operations, including measurements, and on times smaller than the decay or decoherence time.

A system of qubits can be described by a set of coupled $S = 1/2$ spins in a magnetic field. Then the excitation energy of a qubit becomes the Zeeman energy of a spin, whereas the qubit-qubit interaction becomes the exchange spin coupling. Note that the physical interaction itself may be of totally different nature, e.g., electric dipolar or quadrupolar. We will assume that the qubits form a 1D chain.

For many proposed realizations of QC’s [1, 2, 3, 5, 6, 7] the qubit excitation energies are large compared to the interaction. Then the spin-interaction Hamiltonian takes the form

$$H_S = \frac{1}{2} \sum'_{n,m} [J_{nm}^{xx}(S_n^x S_m^x + S_n^y S_m^y) + J_{nm}^{zz}(S_n^z S_m^z)] \quad (1)$$

Here, z is the direction of the effective magnetic field and $J_{nm}^{\mu\mu}$ are the interaction parameters ($\mu = x, y, z$). Only those terms are kept in H_S which, in the Heisenberg representation, do not oscillate at qubit transition frequencies. This is why we have set $J_{nm}^{xx} = J_{nm}^{yy}$. The terms $S_n^x S_m^x + S_n^y S_m^y \equiv (1/2)(S_n^+ S_m^- + S_n^- S_m^+)$ lead to excitation transfer between the qubits n, m provided their energies are close. We note that the spin interaction of the form (1) conserves the number of excitations in the system.

It is convenient to map the spin system onto a system of spinless fermions via Jordan-Wigner transformation [14]. For nearest neighbor coupling, the Hamiltonian of the fermion system becomes

$$H = H_0 + H_i, \quad (2)$$

$$H_0 = \sum_n \varepsilon_n a_n^\dagger a_n + \frac{1}{2} J \sum_n (a_n^\dagger a_{n+1} + a_{n+1}^\dagger a_n),$$

$$H_i = J \Delta \sum_n a_n^\dagger a_{n+1}^\dagger a_{n+1} a_n.$$

Here, a_n^\dagger, a_n are the fermion creation and annihilation operators; they correspond to exciting and de-exciting an n th spin, respectively. The parameter $J = J_{nn+1}^{xx}$ is the fermion hopping integral. The parameter $J\Delta = J_{nn+1}^{zz}$ gives the interaction energy of fermions on neighboring sites. For isotropic Heisenberg coupling of the original spins $\Delta = 1$, but generally $\Delta \neq 1$ in the case of coupled qubits. The on-site fermion energies ε_n are the Zeeman energies of the spins (excitation energies of the qubits) counted off from the characteristic central energy which is the same for all spins inside the chain. For concreteness we set $J, \Delta > 0$.

Localization, and in particular weak localization, is often characterized by the decay of the wave functions of stationary states at large distances. Here we are interested in strong localization. In contrast to weak localization, it is determined by short-range behavior of stationary states and corresponds to their confinement to one or maybe a few neighboring sites.

Strong localization can be conveniently characterized by the inverse participation ratio (IPR), which shows over how many sites the wave function spreads. For an N -particle state λ with wave function $|\psi_{N\lambda}\rangle$ the IPR is given by the expression

$$I_{N\lambda} = \left(\sum_{n_1 < \dots < n_N} |\langle 0 | a_{n_1} a_{n_2} \dots a_{n_N} | \psi_{N\lambda} \rangle|^4 \right)^{-1}, \quad (3)$$

where $|0\rangle$ is the vacuum state. In what follows we will sometimes use the notation $|\psi(k_1, k_2, \dots)\rangle = a_{k_1}^\dagger a_{k_2}^\dagger \dots |0\rangle$ for the wave function (quantum register) in which states k_1, k_2, \dots are occupied and other states are empty. The quantity (3) is also sometimes called the number of participating components, it shows how many matrix elements $\langle \psi(k_1, k_2, \dots) | \psi_{N\lambda} \rangle$ are of order one.

For fully localized states $I_{N\lambda} = 1$. Strong localization means that $I_{N\lambda}$ is close to 1 for all states λ . In this case both the average IPR

$$\langle I_N \rangle = C_{N\lambda}^{-1} \sum_{\lambda} I_{N\lambda}$$

and $I_{N\max} = \max_{\lambda} I_{N\lambda}$ are close to one. Here, $C_{N\lambda}$ is the total number of N -particle states; for an L -site chain $C_{N\lambda} = L! / N!(L-N)!$. Smallness of $\langle I_N \rangle - 1$ is a weaker condition, it is an indication of strong localization of most of the states.

In the opposite limit of extended states we have $\langle I_{N\lambda} \rangle \sim C_{N\lambda} \gg 1$. A simple example are sinusoidal waves in a chain with $\varepsilon_n = \text{const}$, for the case of one particle. For an L -site chain this gives $\langle I_1 \rangle = 2(L+1)/3$ (note that we do not impose periodic boundary conditions, i.e., we consider the so-called “open” chain). The mean IPR sharply increases with the number of particles N , for $N < L/2$.

Strong localization can be also characterized by localization lifetime t_{loc} . This is the time it takes for a localized many-particle state to become resonantly mixed, or hybridized, with another state. If the resonant state into which the system makes a transition is a nearest neighbor, i.e. only one particle has to hop and only to a neighboring site, mixing occurs over time J^{-1} . However, if mixing requires transitions of several particles and/or involves transitions via nonresonant virtual states, it slows down. As we show in Sec. V, the slowing down can be extremely strong for moderately large width of the single-particle energy spectrum.

A. The on-site energy sequence

Localization requires that the on-site energies ε_n be tuned away from each other. The strategy for choosing

the sequence of ε_n while keeping the overall bandwidth of the energy spectrum finite is as follows. First, the energies of nearest neighbors should be moved away from each other. This can be accomplished by separating ε_n into two subbands, with even and odd n , respectively. The distance between the subbands h should significantly exceed the hopping integral J . Then each subband should be further split into two subbands in order to detune next nearest neighbors. The splitting between these subbands can be less than h . This is because next-nearest-neighbor hopping occurs via virtual transitions to a nonresonant nearest-neighbor state, and therefore the effective hopping integral is $\sim J^2/h$. The procedure of band splitting should be continued, and higher-order splittings can be smaller and smaller.

We now introduce a simple sequence of ε_n that implements the structure described above. Except for the energy scaling factor h , this sequence is characterized by one dimensionless parameter α . As we show, it can already be efficient in terms of strong localization. For a semi-infinite chain with $n \geq 1$ we set

$$\varepsilon_n = \frac{1}{2} h \left[(-1)^n - \sum_{k=2}^{n+1} (-1)^{\lfloor n/k \rfloor} \alpha^{k-1} \right], \quad (4)$$

($\lfloor \cdot \rfloor$ is the integer part).

The energy spectrum (4) is illustrated in Fig. 1. The left panel gives the energies of the first 50 sites. It is seen that the states with close ε_n are spatially separated, whereas the states with close n are separated energetically. The multisubband structure of the spectrum is clearly seen in the right panel. For small α , the two major subbands have width $\approx \alpha h$ and are separated by $\approx h$. The splitting of higher-order subbands is of higher order in α . For $\alpha \gtrsim 0.4$ all subbands overlap and the subband structure disappears.

We note that the sequence (4) does not have any simple symmetry. For example, it is not self-similar: the subband widths do not scale with the distance between the sites that belong to the same subband. Nor is the sequence (4) quasi-periodic. However, the coefficients at any given power α^q are repeated with period $2(q+1)$. This important property is essential for obtaining analytical results, see Appendix. As a result of the low symmetry, different subbands in the right panel of Fig. 1 have different numbers of points, i.e., ε_n are not evenly distributed among the subbands. This turns out to be advantageous for strong many-particle localization. The case of a symmetric sequence is discussed in Sec. VI.

An important advantageous feature of the spectrum (4) is that it is convenient for performing gate operations. For single-qubit gates, a single particular radiation frequency can be used to resonantly excite different qubits. It has to be chosen near the average single-qubit transition frequency (which corresponds to $\varepsilon = 0$). Then qubits can be selectively excited by tuning them to this frequency. The transition frequency of the qubit depends on whether neighboring qubits are excited. This can be used for implementing a CNOT gate. Alternatively,

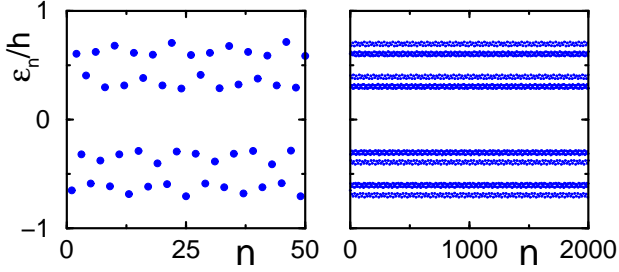


FIG. 1: (color online) The energies ε_n/h for $\alpha = 0.3$. The left panel shows ε_n/h for the sites $n = 1, 2, \dots, 50$. States with close on-site energies are spatially separated. The right panel shows ε_n/h for a much longer array, $n = 1, \dots, 2000$. The energy spectrum displays a multisubband structure, with clearly identifiable 16 subbands in this case.

neighboring qubits can be tuned in resonance with each other, which will lead to a two-qubit excitation swap [13].

III. SINGLE-PARTICLE LOCALIZATION

A. The transition amplitude

Localization of a single particle in tight-binding models with random on-site energies (diagonal disorder) was first studied by Anderson [15]. In 1D all single-particle states are localized, even for weak disorder, and exponentially decay at large distances. Although the sequence (4) is not random, already for not too small α the transition amplitudes also display quasi-exponential decay at large distances provided $J \ll h$, as shown in the Appendix. However, for quantum computing of primary importance is short-range behavior. It turns out that a particle is confined much stronger in the case of the sequence (4) than in the case of random on-site energies distributed within the same energy band, see Sec. VI. The confinement quickly strengthens with the increasing parameter α once α exceeds a certain threshold value α_{th} .

From the viewpoint of decay of single-particle states, it is convenient to characterize an on-site energy sequence by the function

$$K_n(m) = \prod_{k=1}^m J / |2(\varepsilon_n - \varepsilon_{n+k})|. \quad (5)$$

If the states are strongly localized, $K_n(m)$ gives the amplitude of a transition from site n to site $n + m$ [15].

For the sequence (4) in the limit of small α the energy difference $|\varepsilon_{n+m} - \varepsilon_n|$ can be approximated by its leading term, so it is $\sim h$ for odd m and $\sim \alpha h$ for odd $m/2$. In general, the order of the leading term in α increases with increasing m . Still, on the whole the decrease of $|\varepsilon_{n+m} - \varepsilon_n|$ with the increasing intersite distance m is slow.

The asymptotic behavior of the function $K_n(m)$ for small α and large m can be studied rigorously. The anal-

ysis is based on some results of number theory. It is given in the Appendix. It shows that $K_n(m)$ decays with the distance m quasi-exponentially,

$$K_n(m) \propto K^{|m|}, \quad K = \alpha^{-\nu} (J/2h). \quad (6)$$

The exponent ν , and thus the value of K , depend on n and m ; this is why the decay is quasi-exponential, not just exponential. However, the values of ν are bound to a narrow region centered at $\nu = 1$, with $0.89 < \nu < 1.19$. For estimates one can use $\nu = 1$, i.e., set $K = J/2\alpha h$.

Numerical values of ν for different n and m are shown in Fig. 2. They were obtained by keeping the leading term with respect to α in each energy difference $\varepsilon_n - \varepsilon_{n+k}$ with $1 \leq k \leq m$. The data are in excellent agreement with the asymptotic theory.

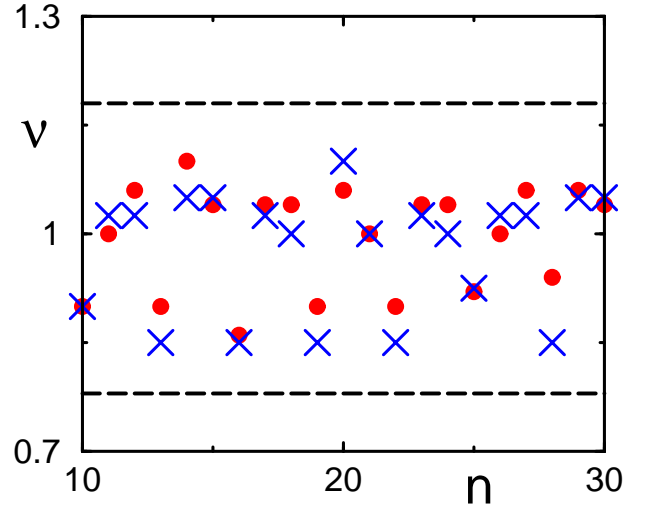


FIG. 2: (color online). The exponent ν of the α -dependence of the transition amplitude $K_n(m)$ for the efficient distance $m = 30$ (crosses) and $m = 50$ (circles) as a function of site number n . The dashed lines show the analytical limits on ν .

Equation (6) gives the tail of the transition amplitude for $J/2\alpha h \ll 1$. It does not immediately describe strong single-particle localization, which is determined by the short-range behavior of the wave function. However, one may expect that strong localization should occur when α becomes much larger than a typical threshold value $\alpha_{\text{th}} = J/2h$. In fact, Eq. (6) describes the transition amplitude only when $\alpha_{\text{th}} \ll \alpha \ll 1$. The condition of strong localization $\alpha_{\text{th}} \ll \alpha < 0.4$, which is necessary to avoid overlapping of the subbands, can be satisfied already for a moderately large ratio of the energy bandwidth h to the hopping integral J .

B. The inverse participation ratio

A quantitative indication of strong localization of single-particle stationary states is that $I_{1\lambda} - 1 \ll 1$. Nu-

numerical results on $\langle I_1 \rangle$ and $I_{1\max}$ as functions of the energy spectrum parameter α for two values of the scaled bandwidth h/J are shown in Fig. 3. They were obtained by diagonalizing the Hamiltonian (1) [or its equivalent (2)] numerically. The data refer to open chains of three different lengths L , with the first site being always $n = 1$ in Eqs. (2), (4). The sum over n in the terms $\propto J, J\Delta$ in Eq. (2) ran from $n = 1$ to $n = L - 1$.

When a transition is made from the spin Hamiltonian (1) to the fermion Hamiltonian (2), the energies ε_n are renormalized. They differ from the transition frequencies of spins by $-J\Delta$ inside the chain. On the boundaries this shift is $-J\Delta/2$. To compensate for this difference, we decreased the transition frequencies of the boundary spins by $-J\Delta/2$, i.e., we added the term $-\frac{1}{2}J\Delta(S_1^z + S_L^z)$ to the spin Hamiltonian (1). Then the interrelation between the spin transition frequencies and the fermion energies ε_n is the same throughout the chain.

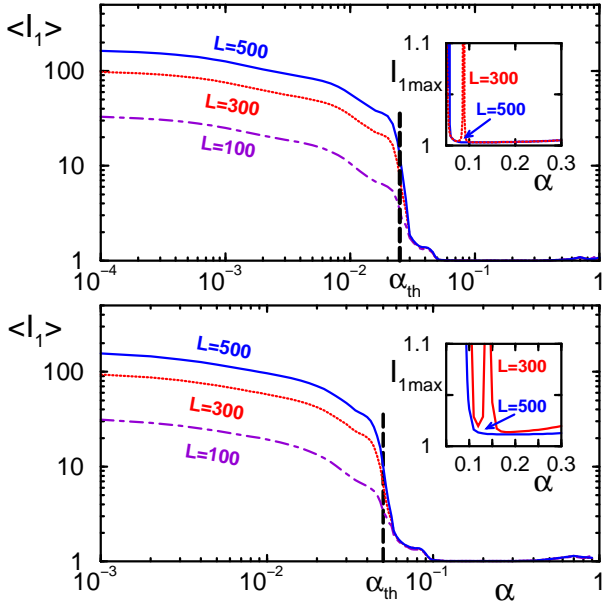


FIG. 3: (color online). The mean single-particle inverse participation ratio $\langle I_1 \rangle$ vs. α for $h/J = 20$ (upper panel) and $h/J = 10$ (lower panel). The data refer to three values of the chain length L . The vertical dashed lines show the analytical estimate for the threshold of strong localization. The insets show the maximal IPR over all states, $I_{1\max} \equiv \max_\lambda I_{1\lambda}$. It sharply decreases with the increasing α . The peak of $I_{1\max}$ for $L = 300$ near $\alpha = 0.1$ is due to the boundary. Near the minimum over α , we have $I_{1\max} \approx 1.01$ for $h/J = 10$, and $I_{1\max} \approx 1.003$ for $h/J = 20$. This demonstrates strong single-particle localization.

In the limit $\alpha \rightarrow 0$, the energies of single-particle states (4) form two bands centered at $h/2$ for even n and $-h/2$ for odd n . For $h \gg J$ the widths of these bands are $\sim J^2/h$. The system is equivalent to two weakly coupled translationally-symmetric chains; the band wave functions are sinusoidal, which gives $\langle I_1 \rangle = (L + 2)/3$. This

agrees with the value of $\langle I_1 \rangle$ for $\alpha \rightarrow 0$ in Fig. 3.

For nonzero α the on-site level detuning (4) breaks translational symmetry. As α increases, the bands at $\pm h/2$ are split, and more and more subbands are resolved in the energy spectrum. Respectively, $\langle I_1 \rangle$ decreases. It sharply drops to ≈ 1 in a narrow region, which can be conditionally associated with a transition to strong localization. The center of the transition region gives the threshold value α_{th} of the parameter α . It appears to be independent of the chain length L . The estimate $\alpha_{th} = J/2h$ from Eq. (6) is in good agreement with the numerical data for different h/J .

When $1 \gg \alpha \gg \alpha_{th}$, all states are strongly localized. Tails of the wave functions are small and limited mostly to nearest neighbors, and $I_{1\lambda}$ is very close to 1.

The dependence of $I_{1\lambda}$ on α is nonmonotonic. The IPR decreases with increasing α for $\alpha < \alpha_{th}$, but for $\alpha \gtrsim 0.4$ the IPR increases with α . This happens because the major bands of ε_n centered at $\pm h/2$ start overlapping. The minimum of the IPR over α is broad for large h/J , and near the minimum $I_{1\lambda} - 1 \approx J^2/h^2$. This estimate is obtained by taking into account the tails of the wave functions on nearest neighbors only. It agrees well with numerical data in Fig. 3. The agreement becomes better with increasing h/J .

The insets in Fig. 3 show that the IPR as a function of α can have narrow resonant peaks. In the presented data they occur for the chain of length $L = 300$. The peaks are seen only in $I_{1\max}$, whereas $\langle I_1 \rangle$ remains close to 1. This indicates that only a few states are hybridized with each other. The underlying resonance results from a different hopping-induced shift of the energy levels at the chain edges compared to the bulk.

The analysis of the wave functions shows that the peak corresponds to a resonance between the sites 300 and 296. Because of the hopping, the energy of the site 300 is shifted by $\approx (J/2)^2/h$, whereas for the site 296 this shift is $\approx J^2/2h$. The difference of ε_n for these sites is $\sim h\alpha^3$ for $\alpha \ll 1$. Then the peak should occur at $\alpha \approx (J/2h)^{2/3}$, in good agreement with the data. The hopping integral between the two states is determined by virtual transitions via intermediate states, it is $\sim J^4/16\alpha h^3$. Therefore the width of the peak with respect to α should be $\propto (J/h)^2$, also in agreement with the data.

We now outline yet another way of looking into the effect of the band structure of the sequence (4) on localization. It is based on varying h/J and finding such energy spectrum parameter α that would keep the IPR constant, i.e.,

$$\langle I_1 \rangle \equiv \langle I_1(\alpha, J/h) \rangle = \text{const.} \quad (7)$$

The average IPR is large, $\approx L/3$, when the spread of the on-site energies ah is small compared to the hopping-induced bandwidth $J^2/2h$ of the bands at $\pm h/2$. When ah becomes comparable to J^2/h , a part of the states become localized with localization length smaller than the chain size, but still there remain states of size $\sim L$. For such states $I_{1\lambda} \propto L$. Their portion depends on

$\alpha h/(J^2/h)$. Therefore one may expect that, for large $\langle I_1 \rangle$ and for a given chain length, α should vary with J/h as $(J/h)^2$.

Another scaling region of $\alpha(J/h)$ as given by Eq. (7) may be expected to emerge for α close to the threshold value, $\alpha_{\text{th}} \lesssim \alpha \ll 1$, but far away from the strong-localization range of α , where $\langle I_1 \rangle - 1 \sim J^2/h^2$.

For α close to α_{th} , the wave functions have comparatively small-amplitude tails that spread over a long distance and are nearly exponential at large distances, as given by Eq. (6). If the decay were purely exponential, i.e., the tail of the wave function centered on site n were of the form $\psi_{n+m} = K^{|m|} \psi_n$, we would have $\langle I_1 \rangle - 1 \approx 4|K|^2$ for $K \approx J/2\alpha h \ll 1$. This condition gives scaling $\alpha \propto J/h$. The nonexponential decay of the wave functions at small to moderate distances (numerically, for $|m| \sim 4-8$) leads to deviations from this simple scaling.

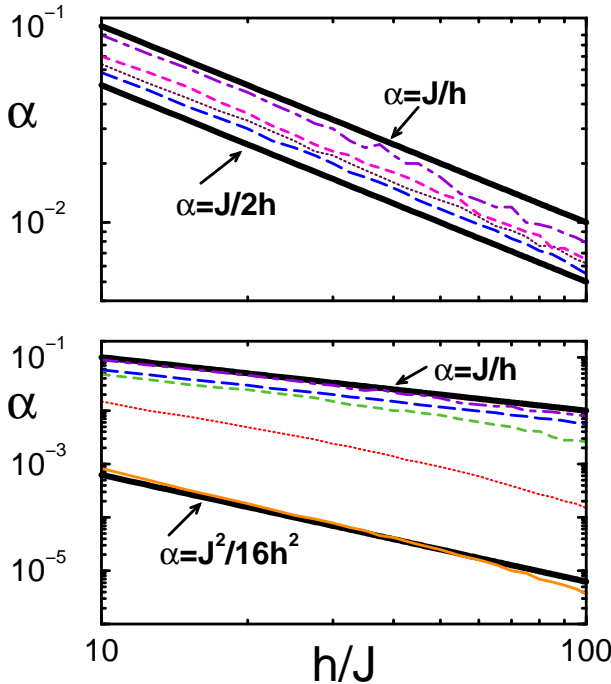


FIG. 4: (color online). The dependence of α on h/J as given by the condition $\langle I_1 \rangle = \text{const}$ for different $\langle I_1 \rangle$ in the chain with $L = 300$. The lines in the lower panel listed from down upward (thin solid, dotted, dashed, long-dashed, and dot-dashed) correspond to $\langle I_1 \rangle = 95, 50, 10, 2$, and 1.2 , respectively. The lines in the upper panel listed from down upwards (long-dashed, dotted, dashed, and dot-dashed) correspond to comparatively small $\langle I_1 \rangle = 2, 1.6, 1.4$, and 1.2 , respectively. The bold lines $\alpha = J^2/16h^2$ and $\alpha = J/h$ display the asymptotic behavior of α for large and small $\langle I_1 \rangle$; the line $\alpha = J/2h$ corresponds to $\alpha = \alpha_{\text{th}}$.

Numerical results on the dependence of α on J/h as given by Eq. (7) are shown in Fig. 4. The data for $\langle I_1 \rangle \sim L/3$ show the expected scaling $\alpha \propto (J/h)^2$. On the other

hand, in the range $\langle I_1 \rangle - 1 \approx 0.1-1$ the value of α scales as J/h . This scaling applies only for $\alpha > \alpha_{\text{th}}$, i.e., for $\alpha h/J > 1/2$. The value of $\alpha h/J$ as given by Eq. (7) increases with decreasing $\langle I_1 \rangle$.

We note that, for large $h/J \sim 100$ and small $\langle I_1 \rangle - 1$, the IPR $\langle I_1 \rangle$ as a function of α displays small oscillations. This leads to multivaluedness of the roots α of the equation $\langle I_1 \rangle = \text{const}$. The roots are numerically very close to each other. We showed the multivaluedness schematically by plotting α vs. h/J in Fig. 4 with jagged lines.

In the intermediate range of $\langle I_1 \rangle$, the function $\alpha(J/h)$ varies from one type of the limiting behavior to the other. In the whole range presented in Fig. 4 both α and J/h are small. However, the numerical data does not seem to suggest that $\langle I_1 \rangle$ has a universal scaling form of a function of $\alpha^{\nu}/(J/h)$ for all $\alpha, J/h \ll 1$.

IV. MANY PARTICLE LOCALIZATION: STATIONARY STATES

A. Many-particle hopping

The localization problem for many-particle states is much more complicated than the problem of single-particle localization. This is a consequence of the interaction between particles, which is formally described by the term $\propto J\Delta$ in the Hamiltonian (2). The case $\Delta = 0$ corresponds to the XY -type coupling between the underlying spins or qubits, when spin excitations on neighboring sites are uncoupled but there is intersite excitation hopping. In this case the single-particle results apply to the many-particle system.

For nonzero Δ , on the other hand, (i) the energy levels ε_n are shifted depending on the occupation of neighboring states, $\varepsilon_n \rightarrow \tilde{\varepsilon}_n$, (ii) there occur combinational many-particle resonances $\tilde{\varepsilon}_{n_1} + \dots + \tilde{\varepsilon}_{n_k} \approx \tilde{\varepsilon}_{m_1} + \dots + \tilde{\varepsilon}_{m_k}$, and as a result, (iii) there occur interaction-induced many-particle transitions that may be resonant even though single-particle resonances have been suppressed. Such transitions may lead to delocalization.

To analyze many-particle effects, it is convenient to change from a_n^\dagger, a_n to new creation and annihilation operators b_n^\dagger, b_n that diagonalize the single-particle part H_0 of the Hamiltonian (2), $a_n = \sum_k U_{nk} b_k$. The unitary matrix \hat{U} is the solution of the equation

$$(U^\dagger H_0 U)_{nm} = \varepsilon'_n \delta_{nm}, \quad (8)$$

$$(H_0)_{nm} = \varepsilon_n \delta_{nm} + \frac{1}{2} J (\delta_{n,m+1} + \delta_{n+1,m}).$$

Here, ε'_n are the exact single-particle energies,

$$U^\dagger H_0 U = \sum_n \varepsilon'_n b_n^\dagger b_n. \quad (9)$$

For $\alpha \gg \alpha_{\text{th}}$ and $J \ll h$, when single-particle states are strongly localized, the energies ε'_n are close to the

on-site energies ε_n . To leading order in J/h , α we have

$$\varepsilon'_n - \varepsilon_n \approx \frac{J^2}{2h} \left[(-1)^n + \frac{1}{2}(-1)^{\lfloor n/2 \rfloor} \alpha \right]. \quad (10)$$

The major term in the right-hand side corresponds simply to renormalization of the characteristic bandwidth of on-site energies $h \rightarrow h + J^2/2h$.

In terms of the operators b_n, b_n^\dagger the interaction part of the Hamiltonian is

$$U^\dagger H_i U = J\Delta \sum V_{k_1 k_2 k_3 k_4} b_{k_1}^\dagger b_{k_2}^\dagger b_{k_3} b_{k_4}, \quad (11)$$

where the sum runs over $k_{1,2,3,4}$, and

$$V_{k_1 k_2 k_3 k_4} = \sum_p U_{pk_1}^* U_{p+1 k_2}^* U_{p+1 k_3} U_{pk_4}. \quad (12)$$

The Hamiltonian (11) describes energy modulation of the exact single-particle excitations by their interaction with each other, as well as direct transitions of excitation pairs.

If the single-particle states are all strongly localized, the off-diagonal matrix elements U_{nk} are small. They are determined by the decay of the wave functions, and therefore fall off exponentially with increasing $|k - n|$. From Eq. (6) we have $U_{nk} \sim K^{|k-n|}$ for $|k - n| \gg 1$. On the other hand, the diagonal matrix element is $U_{nn} \approx 1$.

Therefore, for strong single-particle localization the major terms in the matrix $V_{k_1 k_2 k_3 k_4}$ are those with $\varkappa = 0$, where

$$\varkappa = \min_p (|k_1 - p| + |k_2 - p - 1| + |k_3 - p - 1| + |k_4 - p|). \quad (13)$$

These terms lead to an energy shift $\propto J\Delta$ for the states where particles occupy neighboring sites.

The parameter \varkappa (13) has a simple meaning. It can be seen by noticing that the terms $\propto V_{k_1 k_2 k_3 k_4}$ in Eq. (11) describe two-particle intersite transitions $(k_3, k_4) \rightarrow (k_1, k_2)$ of the renormalized fermions. For a given transition, \varkappa is simply the number of virtual steps that have to be made by the original fermions. The steps are counted off from the configuration where two such fermions occupy neighboring sites, and each step is a transition by one of the fermions to a nearest site.

To make the meaning of \varkappa even more intuitive we give examples of some $\varkappa = 4$ transitions. These are sequences of steps of the original fermions $(n, n+1) \rightarrow (n, n+2) \rightarrow (n-1, n+2) \rightarrow (n-1, n+3) \rightarrow (n-2, n+3)$ or $(n, n+2) \rightarrow (n, n+1) \rightarrow (n, n+2) \rightarrow (n, n+3) \rightarrow (n-1, n+3)$.

It follows from the above argument that, for large \varkappa and $\alpha \gg \alpha_{\text{th}}$, the transition matrix element

$$V_{k_1 k_2 k_3 k_4} \sim K^\varkappa \quad \text{for} \quad \varkappa \gg 1. \quad (14)$$

The transitions of renormalized fermions are not limited to nearest neighbors. However, from Eq. (14), the amplitudes of transitions over many sites are small and rapidly decrease with the number of involved virtual steps. The

overall hopping integral for the renormalized fermions is $VJ\Delta$.

In higher orders of the perturbation theory, the interaction (11) leads also to many-particle transitions. The overall transition amplitude is determined by the total number of involved virtual single-particle steps and falls down as this number increases.

In order to localize many-particle excitations, one has to suppress combinational many-particle resonances keeping in mind that, for localization, the effective hopping integral must be smaller than the energy detuning. This is a hard problem to study analytically, because of the large number of transitions, and we do not have an analytical proof of many-particle localization for our energy sequence (4). Instead we used numerical analysis, as described in the next section, which enabled us to demonstrate strong localization in a chain of a limited size.

B. The inverse participation ratio

As mentioned earlier, a good indicator of strong localization, which applies to both single- and many-particle states, is closeness of the IPR to one. In this section we present numerical data on the IPR obtained by diagonalizing the Hamiltonian (2) in the presence of several excitations. The Hamiltonian is a sparse matrix, which is separated into uncoupled blocks with different numbers of excitations. We focused on the block in the middle of the energy spectrum. For a given chain length L , it has $L/2$ excitations and therefore the largest number of states. This is the worst case, in terms of localization. Chains with $L = 10, 12$, and 14 were studied. The results were similar. We present the data for $L = 12$, in which case the total number of states is 924.

The IPR as a function of the dimensionless parameter α of the on-site energy sequence (4) is shown in Fig. 5. The results refer to two values of the dimensionless ratio of the hopping integral to the interband distance J/h and several values of the dimensionless parameter of the particle interaction Δ .

We start the analysis with the region $\alpha \rightarrow 0$, where the on-site energies (4) alternate between $\pm h/2$. For large h/J the levels are broadened into well-separated single-particle bands of width $J^2/2h$. In the neglect of band mixing, the many-particle wave functions can be found using the Bethe ansatz. For $\Delta = 0$ the energy spectrum consists of bands that are determined by the number of particles in each of the two single-particle bands. Because each of the many-particle bands has many states, the IPR is large, with $\langle I_6 \rangle \approx 78$ for $h/J = 20$ and $L = 12$, see Fig. 5.

For $\alpha \rightarrow 0$ the IPR should decrease with the increasing parameter of the particle interaction Δ until it saturates as a function of Δ . This happens, because for large $\Delta \gg J/h$ (but $\Delta \ll h/J$) the energy bands at $\pm h/2$ split into subbands depending on the number of particle pairs,

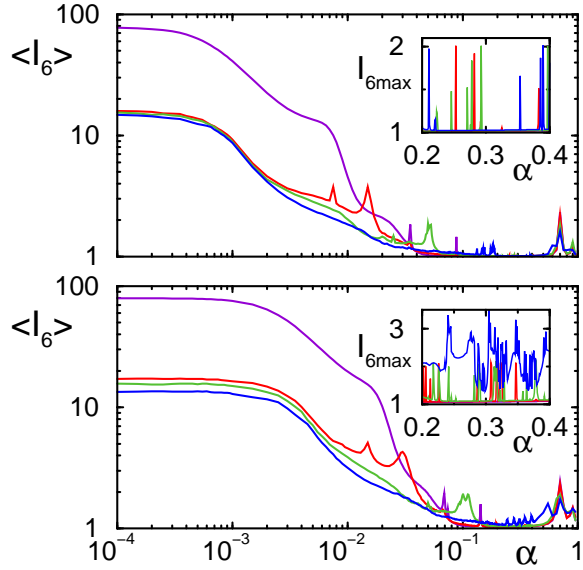


FIG. 5: (color) The IPR for 6 excitations on the first 12 sites of the chain (4). The reduced bandwidth of the energy spectrum is $h/J = 20$ (top panel) and $h/J = 10$ (lower panel). The purple, red, green, and blue curves refer to the coupling parameter $\Delta = 0, 0.3, 1$, and 3 , respectively. The peaks of $\langle I_6 \rangle$ for $\Delta = 0$ are due to boundary-induced resonances of single-particle energies. The insets show the maximal I_6 for $\Delta \neq 0$. Sharp isolated peaks of $I_{6\max}$ vs α result from the hybridization of resonating many-particle states.

triples, etc. on neighboring sites: for example, the energy of a pair on neighboring sites differs from the energy of a dissociated pair by $J\Delta$. Since the number of states in a subband is smaller than in the whole band, such splitting reduces the average IPR.

The decrease of the average IPR with increasing Δ for $\alpha \rightarrow 0$ and $\Delta \ll h/J$ is seen in Fig. 5. We note that the mere separation (by h) of the single-particle energies of neighboring states is not sufficient for reaching strong localization, even with account taken of the particle-particle interaction. Inside each subband, the number of resonating states in a long chain is still very large. Localization requires that not only nearest neighbor single-particle energies, but also energies of remote sites be tuned away from each other, which happens for sufficiently large values of the parameter α in Eq. (4).

This argument is confirmed by the data in Fig. 5. For given Δ , the IPR decreases as a whole with increasing α in the range where the single-particle bands are well separated, $\alpha \lesssim 0.4$. This is the expected consequence of eliminating energy resonances.

For $\Delta \leq 1$, in the region $0.2 \lesssim \alpha \lesssim 0.4$, except for narrow peaks, we have $I_{6\max} \approx 1.09$ for $h/J = 10$ and $I_{6\max} \approx 1.02$ for $h/J = 20$. The values of $\langle I_6 \rangle$ are even smaller, 1.04 and 1.01, respectively. This indicates that, in this parameter range, all states are strongly localized. For $\Delta = 3$ and $h/J = 20$ we also have $I_{6\max} \approx 1.01$

away from the peaks; however, for $h/J = 10$ there occur resonances, which are discussed below.

C. Narrow resonances of the IPR

A distinctive feature of the many-particle IPR as function of α is the onset of multiple resonant peaks, which can be seen in Fig. 5. They indicate that at least some of the states are no longer strongly localized. The peaks are due to inter-state resonances and the hybridization of resonating states. The hybridization occurs when the matrix elements of interstate transitions in Eqs. (11), (12) exceed the energy difference of the states. For $0.2 \lesssim \alpha \lesssim 0.4$, i.e., in the region of strong localization, and for $h/J = 20$ and chosen $\Delta \leq 3$ we found that only two states could become strongly hybridized. For a larger number of states hybridization was small. This leads to $I_{6\max} \lesssim 2$. For $h/J = 10$ and $\Delta = 3$ the interstate coupling (12) is stronger, and as a result three states can be strongly hybridized and a few more can be weakly admixed, leading to $I_{6\max} \sim 3$ at resonant α .

Because the interaction is two-particle, the strongest peaks of $I_{6\max}$ come from resonances that directly involve two particles (the hybridization of three states mentioned above is a result of such resonances, too). They occur when the energy difference

$$\delta\varepsilon = |\varepsilon_{k_1} + \varepsilon_{k_2} - \varepsilon_{k_3} - \varepsilon_{k_4}| \quad (15)$$

is close to $MJ\Delta$ with $M = 0, 1, 2$. Strictly speaking, we should use exact single-particle energies ε'_n (9) instead of ε_n in Eq. (15), but the difference between these energies is small, see Eq. (10), and it leads to a small shift of the positions of the resonances discussed in this section.

As we increase α starting from $\alpha = 0$, pronounced peaks of $\langle I_6 \rangle$ appear for

$$\delta\varepsilon \approx sah \approx J\Delta$$

with $s = 1, 2$. They are due to resonant hybridization of pairs on neighboring sites $(n, n+1)$ with dissociated pairs located on sites $(n, n+3)$ for $s = 1$, and $(n-1, n+2)$ with even n for $s = 2$, for example. Such hybridization corresponds to $\varkappa = 2$. A specific example for the studied chain with $\Delta = 1$, $h/J = 20$, and $\alpha = 0.05$ is the resonance between the states $|\psi(3, 4, 6, 7, 8, 9)\rangle$, $|\psi(4, 5, 6, 7, 8, 9)\rangle$, $|\psi(3, 4, 6, 7, 8, 11)\rangle$ and $|\psi(4, 5, 6, 7, 8, 11)\rangle$ (we remind that the arguments of ψ indicate the positions of the excitations; we have six excitations, and the available sites are $1, 2, \dots, 12$). All these states can be obtained from each other by moving one excitation by two positions. For example, in the first pair the excitation goes from site 3, where it has one nearest neighbors, to site 5, where it has two neighbors.

The width of the above peaks $\delta\alpha$ can be estimated from the condition that the frequency detuning $|sah \pm J\Delta|$ is of order of the effective hopping integral $J\Delta V_{k_1 k_2 k_3 k_4}$. For $s = 1$ [an $(n, n+1) \rightarrow (n, n+3)$ -type transition]

the hopping integral is $\sim J^3 \Delta / \alpha h^2$ from Eqs. (11), (12). This gives the width

$$\delta\alpha \sim (J/h)^2.$$

The positions of the peaks $\alpha \approx J\Delta/sh$ and their widths are in agreement with the data in both upper and lower main panels of Fig. 5.

For larger α , narrow resonances with respect to α occur when

$$s\alpha^m h \approx MJ\Delta$$

with integer s, m, M , and $m \geq 2, M \geq 1$. They may happen, for example, between pairs $(n, n+1)$ and $(n-1, n+2)$ with odd n such that $n \neq 3k-1$, in which case $m=2$ and $\varkappa=2$. A specific example for our chain is the resonance between the states $|\psi(1, 3, 4, 6, 9, 11)\rangle$ and $|\psi(1, 2, 5, 6, 9, 11)\rangle$ for $\Delta=1, h/J=20$, and $\alpha=0.246$. Here the excitations on sites $(3, 4)$ move to sites $(2, 5)$, and $\alpha^2 h \sim J\Delta$ (in fact, higher-order terms in α are essential for fine-tuning the states into resonance). In other cases resonances with $m \geq 2$ require more intermediate virtual steps, with $\varkappa \geq 4$.

The $m \geq 2$ -resonances are extremely narrow for $\alpha_{\text{th}} \ll \alpha \ll 1$. For example, for $m=2$ their widths are

$$\begin{aligned} \delta\alpha &\lesssim (J/h)^{5/2} \Delta^{1/2} \quad \text{for } \varkappa=2, \\ \delta\alpha &\lesssim J^3/h^3 \Delta \quad \text{for } \varkappa=4. \end{aligned}$$

In these estimates we used that, from Eqs. (4), (12) $|V_{n-1, n+2, n, n+1}| \lesssim J^2/h^2$ for the $\varkappa=2$ -transition $(n, n+1) \rightarrow (n-1, n+2)$. For the $m=2$ and $\varkappa=4$ -transitions, on the other hand, $|V_{k_1, k_2, k_3, k_4}| \lesssim J^4/\alpha^3 h^4$ [for example, this estimate applies to a transition $(n, n+1) \rightarrow (n, n+5)$]. We note that, from the condition $\alpha_{\text{th}} \ll \alpha$ and the resonance condition $s\alpha^2 h = MJ\Delta$, it follows that $\Delta \gg J/h$, which guarantees the smallness of the peak widths.

Each high-order resonance gives rise to a narrow band of resonant α values. All of them refer to a resonant transition between the same sites. However, the energy difference of these sites is slightly different depending on the occupation of remote sites, for example, next nearest neighbors. In this latter case, from Eqs. (11), (12), the corresponding shift of α is $\propto (J/h)^{5/2} \Delta^{1/2}$.

A specific example for the studied chain is provided by the resonances between two pairs of states, $|\psi(2, 3, 6, 7, 8, 12)\rangle$ and $|\psi(2, 3, 6, 8, 11, 12)\rangle$, on the one hand, and $|\psi(5, 6, 7, 8, 9, 12)\rangle$ and $|\psi(5, 6, 8, 9, 11, 12)\rangle$, on the other hand. In both cases the resonant transition is fermion hopping from site 7 to site 11. Both resonances occur for $\Delta=1, h/J=20$, but the first corresponds to $\alpha \approx 0.2778$, whereas the second corresponds to $\alpha \approx 0.2782$. The difference in α comes primarily from the different occupation of the next nearest neighbors of sites 7 and 11.

The most pronounced peaks in Fig. 5 correspond to comparatively small $\varkappa \leq 4$. However, there are resonances for higher \varkappa as well. The resonating energies have

to be extremely close to each other for such states to be hybridized. The corresponding peaks are very narrow, and very high precision is needed to find them numerically (sometimes the hybridization appears to be an artifact of not sufficiently precise calculations).

As mentioned above, in the region $0.2 \lesssim \alpha \lesssim 0.4$ the positions of the IPR peaks are determined not only by the leading-order terms in α , but also by higher-order terms. Therefore there are several resonant bands for each s, m, M as given by the condition $s\alpha^m \approx MJ\Delta$. This explains why there are several bands in Fig. 5. These bands are well separated for sufficiently large h/J and not too large Δ . On the other hand, for $h/J=10$ and $\Delta=3$ the bands of resonances are broadened and overlap with each other.

D. Broad-band two-particle resonances

A special role in the problem of many-body localization is played by two-particle resonances that are not selective in α , i.e., exist in a broad range of α . For these broad-band resonances, the total energy difference between the initial and final states is small, $\delta\varepsilon \ll J$. They emerge already in the second order in J/h (i.e., $\varkappa=2$) for pairs $(n, n+1)$ and $(n-1, n+2)$, i.e.,

$$\varepsilon_n + \varepsilon_{n+1} \approx \varepsilon_{n-1} + \varepsilon_{n+2}. \quad (16)$$

If n and $n+2$ are prime numbers, the energy difference $\delta\varepsilon = |\varepsilon_n + \varepsilon_{n+1} - \varepsilon_{n-1} - \varepsilon_{n+2}| \sim \alpha^{n-1} h$ is extremely small for large n .

More generally, the resonance (16) occurs for all $n = 6k-1$ with integer k . In this case $\delta\varepsilon/h \propto \alpha^\xi$ with $\xi \geq 4$. Such $\delta\varepsilon$ is “anomalously small” for $\varkappa=2$. The hopping integral $J^3\Delta/h^2$ becomes larger than $\delta\varepsilon$ even when we are already deep in the single-particle localization region $\alpha \gg \alpha_{\text{th}}$. It can be shown that, to leading order in J/h , the corresponding energy difference of renormalized energies ε'_n differs from $\delta\varepsilon$ only by $(J^2/h)\alpha^3$, which can also be much smaller than $J^3\Delta/h^2$. More many-particle broad-band resonances emerge for higher \varkappa .

For the section of the chain with sites $1 \leq n \leq 12$ the IPR is not much affected by the above resonances, because even where n and $n+2$ are prime numbers (5 and 7), they are not very large and the energy difference (16) is not exceedingly small.

To better analyze the effects of the resonances (16), we computed the IPR for different sections of the chain (4) with $n_0 \leq n \leq n_0 + 11$ and different n_0 . We found that the resonances increase $\langle I_6 \rangle$ up to 1.15, for $h/J=20$, $0.2 < \alpha < 0.4$, and $\Delta=1$.

For a finite chain, the resonances can be eliminated order by order in \varkappa by shifting the energies of appropriate qubits. A simple systematic modification of the energies that works for $\varkappa \leq 5$ is discussed in the next section, see Eq. (18). This modification brings the IPR back to smaller values. For example, in all sections of the chain that we studied it made $\langle I_6 \rangle$ and $I_{6\text{max}}$ equal to ≈ 1.01

and ≈ 1.02 , respectively, which are the values we had for the section $1 \leq n \leq 12$. This indicates that the localization of stationary states for the energy sequence (18) is very strong.

V. LIFETIME OF STRONGLY LOCALIZED STATES

The problem of strong localization can be viewed also from a different perspective. In the context of quantum computing, it suggests a more appropriate formulation than the formulation based on the analysis of stationary states. It is also relevant for condensed-matter systems.

First we note that qubit states have a finite coherence time t_{coh} . This time has to be compared with the reciprocal time of a single- or two-qubit operation in a quantum computer. For systems that we study the duration of a two-qubit operation is limited by resonant excitation transfer between the qubits. Therefore it is $\gtrsim J^{-1}$. This means that the clock frequency is $\lesssim J$. In most proposed realizations of a QC the coherence time exceeds the gate operation rate by a factor $\lesssim 10^5 - 10^6$.

We define the localization lifetime t_{loc} as the time it takes for excitations to leave occupied sites. Clearly, in the quantum computing context, localization of excitations is only relevant on times $\sim t_{\text{coh}}$. Then to have strong localization it suffices that $t_{\text{loc}} \gtrsim t_{\text{coh}}$. It follows from the estimate for t_{coh} that the latter condition is met if

$$t_{\text{loc}} \gtrsim 10^5 - 10^6 J^{-1}. \quad (17)$$

The condition (17) must be satisfied for all many-excitation states. It is this condition that imposes a constraint on the form of the energy sequence ε_n .

In order to estimate t_{loc} for the energy sequence (4) we note that, once nearest-neighbor resonances have been eliminated, t_{loc} is determined by resonant transitions to remote sites. They occur via virtual transitions to nonresonant states. For a two-particle resonant transition, the minimal number of the needed virtual transitions is given by the parameter \varkappa (13). Then from Eqs. (11), (14) the hopping integral for a resonant transition $(k_3, k_4) \rightarrow (k_1, k_2)$ is

$$J\Delta V_{k_1 k_2 k_3 k_4} \sim J\Delta K^{\varkappa}$$

for $\varkappa \gg 1$. Here, K is defined by Eq. (6), $K \approx J/2\alpha h$, and $K \ll 1$ in the region $\alpha/\alpha_{\text{th}} \gg 1$.

The localization lifetime t_{loc} is determined by the minimal reciprocal hopping integral, with the minimum taken with respect to all resonating many-excitation states. For two-particle transitions $t_{\text{loc}} \sim [J\Delta K^{\varkappa_{\text{min}}}]^{-1}$, where \varkappa_{min} is the smallest value of \varkappa for which the initial and final states of the system may be in resonance.

To have $t_{\text{loc}}J$ that exceeds a given value, we must have an appropriate \varkappa_{min} . This means that we should eliminate resonances between all states connected by

$\varkappa < \varkappa_{\text{min}}$ virtual transitions. For a moderately narrow energy bandwidth, where $K \sim 0.1$, and for the coupling parameter $\Delta \lesssim 1$ we will have $t_{\text{loc}}J \gtrsim 10^6$ already for $\varkappa_{\text{min}} = 6$. In fact, this gives an underestimate of $t_{\text{loc}}J$, because the hopping integral for transitions with $\varkappa = 6$ is limited by $\sim J\Delta(J/h)^6\alpha^{-5}$ rather than $J\Delta(J/h)^6\alpha^{-6}$, as would be expected from the asymptotic expression (14).

To obtain $\varkappa_{\text{min}} = 6$ we have to eliminate all resonances to 5th order, i.e., for $\varkappa \leq 5$. For $h \gg J, J\Delta$ and $\alpha \ll 1$ there are no many-particle 5th order resonances, because the difference of the on-site energies is $\sim h$. From Eq. (11), the 4th order resonances can occur only for two-particle transitions. Therefore the change of the interaction energy is limited by $2J\Delta$.

The 4th order resonances will be eliminated if the detuning of the on-site energy differences $\delta\varepsilon$ for all corresponding transitions is

$$\delta\varepsilon > 2J\Delta.$$

This means that we have to open a zero-energy gap of an appropriate width in $\delta\varepsilon$. We note that this is a sufficient, not the necessary condition: in principle, it would suffice to have narrow gaps at $\delta\varepsilon = 0, J$, and $2J$. For a specific finite-length section of a chain this may be more practical. However, here we are interested in an infinite chain, and we want to demonstrate that even for such a chain all resonances can be eliminated.

To create the zero-energy gap the sequence (4) has to be modified. The modification has to eliminate, in the first place, the “anomalous” broad-band resonances for transitions $(n, n+1) \rightarrow (n-1, n+2)$ with $n = 6k-1$ discussed before. This will, of course, also eliminate resonances where n and $n+2$ are prime numbers. Such modification is a shift of ε_n for each $n = 6k$ with integer s , i.e., for each 6th site. An even better result can be obtained if we shift the energy of every 3rd site, $n = 3k$, as in this case we will eliminate all resonances of order $\delta\varepsilon \propto \alpha^3$, to leading order in α . For example, we have $\delta\varepsilon \propto \alpha^3$ for a transition $(n-1, n) \rightarrow (n-1, n+4)$ with $n = 3k-1$; we note that in this case the renormalization $\varepsilon_n \rightarrow \varepsilon'_n$ leads to the change $\delta\varepsilon \propto (J^2/h)\alpha^3$.

A simple modification that eliminates broad-band resonances up to 4th order has the form

$$\varepsilon_n^{\text{md}} = \varepsilon_n - (h/2)\beta(-1)^k \quad \text{for} \quad n = 3k, \quad (18)$$

while $\varepsilon_n^{\text{md}} = \varepsilon_n$ for $n \neq 3k$. Eq. (18) corresponds to shifting ε_{3k} up or down by $\beta h/2$ depending on whether s is odd or even.

The values of the parameter β should be much larger than α^3 , to open an appreciable gap, but smaller than α to avoid creating new resonances between qubits coupled in second order in J .

The onset of a zero-energy gap in energy differences as a result of the modification (18) is seen in Fig. 6. The figure shows the low-energy parts of the modified energy differences

$$\delta\varepsilon_{k_1}^{\text{md}} = |\varepsilon_{k_1}^{\text{md}} + \varepsilon_{k_2}^{\text{md}} - \varepsilon_{k_3}^{\text{md}} - \varepsilon_{k_4}^{\text{md}}|$$

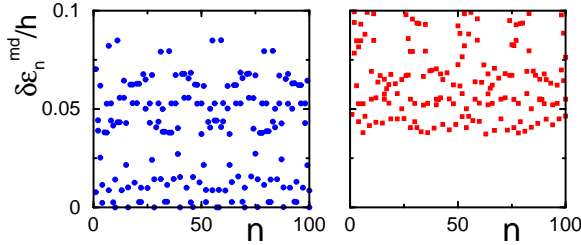


FIG. 6: (color online) The low-energy part of the modified energy differences $\delta\epsilon_n^{\text{md}}/h$ for all transitions with $\varkappa \leq 4$ in which one of the involved particles is initially on the n th site. The data refer to $\alpha = 0.23$. The left panel corresponds to the original sequence (4), i.e., $\beta = 0$ in Eq. (18). The right panel refers to the sequence (18) with $\beta = 0.11$.

[cf. Eq. 15)] as a function of the initial position k_1 of one of the particles involved in the transition (we assume that the initial position of the other particle $k_2 > k_1$). We plot $\delta\epsilon_{k_1}^{\text{md}}$ for all two-particle transitions $(k_1, k_2) \rightarrow (k_3, k_4)$ with $\varkappa \leq 4$, where \varkappa for given $k_{1,2,3,4}$ is given by Eq. (13). The total number of potentially resonant transitions with $\delta\epsilon/h \lesssim \alpha^2$ for small α is equal to 6.

The left panel in Fig. 6 shows that, for the initial sequence (4), there is no gap in the values of $\delta\epsilon$ at low energies. The right panel demonstrates that, with a correction (18), we can open an appreciable zero-frequency gap. The gap depends on the values of α and β , but this dependence is smooth. For the specific parameter values in Fig. 6 we have $\delta\epsilon \geq 0.037$. We have checked that the gap persists for a much longer chain, with n from 1 to 10,000. This means that localized many-particle states will have a lifetime $\gtrsim 10^6 J^{-1}$ for $2J\Delta/h < 0.037$.

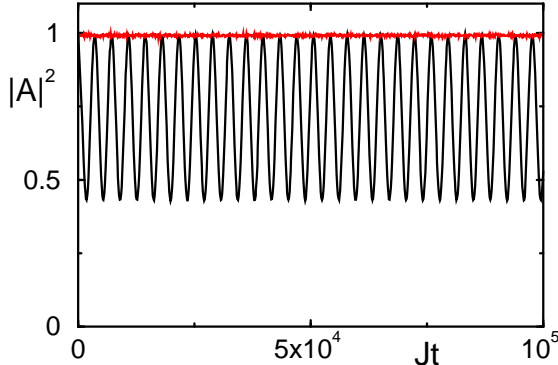


FIG. 7: (color online) Time evolution of the squared amplitude $|A|^2$ of the state $|\psi(416, 419, 420, 422, 423, 424)\rangle$ in a 12-site section of the chain between $n = 415$ and $n = 426$. The oscillating line refers to the original sequence (4) with $\alpha = 0.23$. The nearly constant line refers to the modified sequence (18) with $\alpha = 0.23, \beta = 0.11$. In both cases $h/J = 20$ and $\Delta = 1$.

Fig. 7 illustrates strong localization for the

modified energy sequence (18). In the case of the original sequence (4), the chosen state $|\psi(416, 419, 420, 422, 423, 424)\rangle$ strongly hybridizes with the state $|\psi(416, 418, 421, 422, 423, 424)\rangle$ for all α of physical interest, $\alpha < 0.4$. This happens because the difference of single-particle energies $\epsilon_{419} + \epsilon_{420}$ and $\epsilon_{418} + \epsilon_{421}$ is $\propto \alpha^{4/8}$. The hybridization results in oscillations of the amplitude of the state, as seen from Fig. 7. For the modified sequence (18) the resonance is eliminated, and the amplitude remains constant over a time $> 10^6 J^{-1}$, as expected.

A. Stability with respect to errors in on-site energies

In a real system, it will be impossible to implement the sequence of on-site energies (4) precisely. This is because these energies contain high powers of the small parameter α , while the precision to which they can be determined is limited. Therefore it is necessary to study localization in the presence of errors in ϵ_n and to find how large these errors can be before they cause delocalization.

We will address this problem by looking at the gap in the energy differences $\delta\epsilon$ in the presence of errors in ϵ_n^{md} (18). As long as this gap remains larger than $2J\Delta$ for all resonant transitions with $\varkappa \leq 5$, the localization lifetime t_{loc} will remain large and will satisfy the inequality (17).

The effect of errors on the gap can be modelled by adding a random term to on-site energies, i.e., replacing ϵ_n^{md} with

$$\epsilon_n^{\text{err}} = \epsilon_n^{\text{md}} + \frac{1}{2}Dhr_n. \quad (19)$$

Here, r_n are random numbers uniformly distributed in the interval $(-1, 1)$, and D characterizes the error amplitude. It should be compared with α^s with different exponents $s \geq 1$. When $D \sim \alpha^s$ it means that the energies ϵ_n are well controlled up to terms $\sim \alpha^{s-1}$, to leading order in α .

The results on the gap $\delta\epsilon$ as a function of $\log D$ are shown in Fig. 8. The gap is calculated for two-particle transitions with $\varkappa \leq 4$, as in Fig. 6. In the lower panel the gap is scaled by its value in the absence of errors,

$$R = \min_n \delta\epsilon_n^{\text{err}} / \min_n \delta\epsilon_n^{\text{md}}. \quad (20)$$

The data refer to the same α, β as in Fig. 6.

It is seen from Fig. 8 that, for the chosen α, β the gap remains unchanged for $D \lesssim \alpha^4$. This is because, for the modified energies ϵ_n^{md} , the terms $\sim \alpha^3$ drop out from the energy differences that we discuss. For $D = \alpha^3$ the gap is reduced, but only slightly. For $D = \alpha^2$ it becomes significantly smaller than for $D = 0$, and it ultimately disappears with increasing D .

The results of Fig. 8 demonstrate that the localization persists even for relatively large errors in the on-site energies. At least for the chosen α, β errors in ϵ_n up to $\sim 1.2\%$

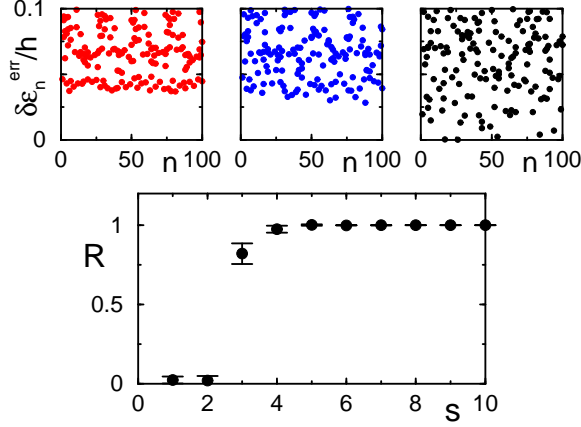


FIG. 8: (color online) Upper panels: all energy differences $\delta\epsilon_n^{\text{err}}/h = |\epsilon_n^{\text{err}} + \epsilon_{n_1}^{\text{err}} - \epsilon_{n_2}^{\text{err}} - \epsilon_{n_3}^{\text{err}}|/h$ for transitions $(n, n_1) \rightarrow (n_2, n_3)$ that correspond to the number of intermediate steps $\kappa \leq 4$. The data refer to $\alpha = 0.23$, $\beta = 0.11$, and to a specific realization of the random numbers r_n in Eq. (19). The boxes from left to right correspond to the values of the noise intensity D in Eq. (19) $D = \alpha^s$ with $s = 4, 3$, and 2 . Lower panel: the scaled minimal gap R (20) as a function of the logarithm $s = \log D / \log \alpha$. Error bars show the standard deviation of R .

(when $D = \alpha^3$) lead only to an insignificant change in the width of the energy gap. They will make no effect on the localization lifetime provided the gap exceeds $2J\Delta$.

The observed dependence on the noise strength suggests that, in the presence of noise, the sequence (4), (18) can be cut so that the terms $\propto \alpha^s$ with $s > s_{\text{cutoff}}$ are disregarded. The value of s_{cutoff} depends on the noise, $s_{\text{cutoff}} = \ln D / \ln \alpha$. TAs a result of the cutoff, the energies ϵ_n become polynomials in α of power $\leq s_{\text{cutoff}}$. From Eq. (4), these polynomials are periodic in n , with the period determined by twice the least common multiple of $(2, 3, \dots, s_{\text{cutoff}} + 1)$. For example, for $s_{\text{cutoff}} = 4$ the period in n is 120 (see also Appendix). For such a long period and short-range hopping, even a small disorder $\propto D$ must be sufficient to localize excitations or at least make them stay on their sites for a long time.

VI. ALTERNATIVE ENERGY SEQUENCES

Neither the original sequence of on-site energies (4) nor its modified version (18) were optimized to maximize the IPR or the localization lifetime. Therefore it is important to compare them with other sufficiently simple sequences. This will be done in this section for two natural choices of ϵ_n .

A. Period doubling cascade

A simple way to move sites with close energies far away from each other is to make the energies form a “period doubling cascade” (PDC). It is described by a one-parameter energy sequence, and in what follows h is the energy scale and α is the parameter.

In the PDC, the on-site energies are first split into two subbands, with nearest neighbors being in different subbands, but next nearest neighbors being in the same subband. The subbands differ in energy by $\alpha^0 h$, to leading order in α [this is also the case in Eq. (4)]. Each of the subbands is then further split into two subbands of 4th neighbors. The leading term in the energy difference of these subbands is $\alpha^1 h$. Each subband is then split again into two subbands of 8th neighbors. The leading term in their energy difference is $\alpha^2 h$. This period-doubling process is then continued indefinitely, for an infinite chain.

The expression that describes the on-site energy sequence for the PDC, ϵ_n^{PDC} , can be conveniently written in terms of the coefficients $j_k(n) = 0, 1$ of the expansions of site numbers n in base two,

$$n = \sum_{k=0}^{M(n)-1} j_k(n) 2^k.$$

Here, $M(n) = 1 + \lfloor \log_2 n \rfloor$ is the number of integer digits of n in base 2.

We set

$$\epsilon_n^{\text{PDC}} = \frac{1}{2} h \left[(-1)^n + \sum_{k=1}^{M(n)-1} (-1)^{j_k(n)} \alpha^k \right]. \quad (21)$$

The energies ϵ_n^{PDC} are shown in Fig. 9. It is instructive to compare this figure with Fig. 1 for the energies (4). The overall band structure is similar, but the energy distribution is much more regular for the PDC. For example, it is seen from the panels for 2000 sites that the minibands for the PDC sequence are equally populated. However, as we show later, the symmetry of the PDC is actually bad from the viewpoint of many-particle localization.

Spatial separation of states with close on-site energies in the PDC leads to effective single-particle localization. As in the case of the sequence (4), the values of $\langle I_1 \rangle - 1$ are $\sim 3 \times 10^{-3}$ for $h/J = 20$ near the minimum of $\langle I_1 \rangle$ over α . This minimum is located at $\alpha \approx 0.1$.

The situation is different for many-particle localization. Here the high symmetry of the PDC leads to multiple many-particle resonances. For example, two-particle states $(n, n+1)$ and $(n-1, n+2)$, which are coupled in second order in J/h , have exactly same energies whenever n is odd. The states $(n, n+1)$ and $(n-2, n+3)$, that are coupled in the fourth order in J/h , have same energies when $n = 7 + 4k$ with integer k . We note that there were no exactly degenerate states for the sequence (4), and the portion of two-particle states with close energies was much smaller. Therefore it is more complicated to find

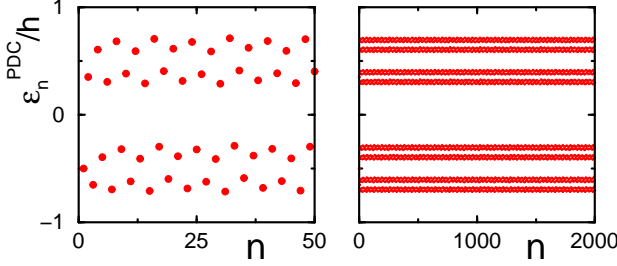


FIG. 9: (color online) The on-site energies $\varepsilon_n^{\text{PDC}}/h$ (21) for $\alpha = 0.3$. The left panel shows the energies for the sites $n = 1, 2, \dots, 50$. States with close on-site energies are spatially separated. The right panel shows $\varepsilon_n^{\text{PDC}}/h$ for a much longer array, $n = 1, \dots, 2000$. The energy spectrum displays a multisubband structure. Because of the symmetry of the sequence (21), the number of points in each subband is approximately the same, in contrast to the sequence (4), cf. Fig. 1.

a correction to the sequence (21) that would eliminate many-particle resonances. As a result, unexpectedly, this symmetric sequence is less convenient from the point of view of strong localization.

B. Random on-site energies

The case opposite to the highly symmetric sequence (21) is when the on-site energies ε_n are completely random. It is well-known that such randomness leads to single-particle localization in a 1D chain. However, it does not lead to strong localization of all states, because there is always a nonzero probability to have nearest neighbors with energies that differ by less than J and therefore are hybridized. As explained in the Introduction, hybridization is even more likely to happen in the case of many-particle states, because it is more likely to have neighboring nearly resonant states.

A simple random sequence of on-site energies has the form

$$\varepsilon_n^r = W r'_n, \quad (22)$$

where r'_n with different n are independent random numbers uniformly distributed in the interval $(0, 1)$, and W is the bandwidth. The results on the IPR for the sequence (22) are shown in Fig. 10.

Localization of stationary states for the random sequence (22) can be characterized by the probability distribution of the IPR $P(I)$. This distribution is obtained by numerically diagonalizing the Hamiltonian (2) for different realizations of the on-site energies (22).

As seen from Fig. 10, both single- and many-particle IPR distributions display peaks near $I = 1$. This indicates that, for the broad energy bandwidths used in the calculations, the stationary states of the system are most likely localized. However, the distributions are broad and

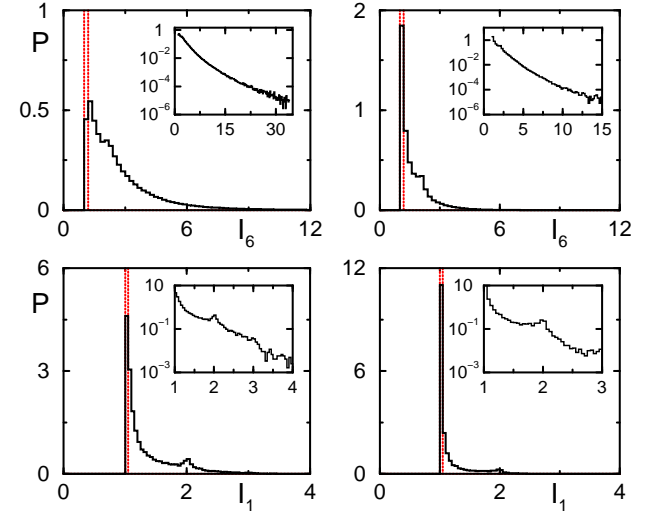


FIG. 10: (color online) The normalized distributions of the IPR $P(I)$ for the random energy sequence (22). The upper and lower panels refer to the many- and single-particle IRS: 6 excitations with $\Delta = 1$ in the chain of length $L = 12$ and one excitation in the chain of $L = 300$, with 2000 and 80 realizations, respectively. The left and right panels refer to the overall bandwidth of the on-site energy spectrum $W/J = 13$ and 26. The narrow columns at $I = 1$ showed with dotted lines refer to the sequence (4), with $h/J = 10$ and 20 for the left and right panels, respectively. The values of α in Eq. (4) were chosen so as to have the same bandwidths of on-site energies as the corresponding random sequences: in the lower panels $\alpha \approx (W - h)/W \approx 0.231$ (as in an infinite chain), whereas in the upper panels $\alpha = 0.274$ to allow for a comparatively small number of sites. The insets show $\log P$ vs. I .

slowly decay on the tails. This means that many states are strongly hybridized, that is the stationary wave functions spread over several sites, which could be explained by multiple resonances. The insets in Fig. 10 show that, at least for not too large I , the tails of $P(I)$ are non-exponential. They rather display a power-law behavior.

The typical distribution width decreases with the increasing bandwidth W of on-site energies. As expected, the distributions of many-particle IPRs (the upper panels in Fig. 10) are much broader and their peaks near $I = 1$ are much smaller than for the single-particle distributions (the lower panels).

The IPR distributions for the random sequence (22) differ dramatically from the distributions for the regular sequence (4). The latter are narrow and concentrate in a small region of I close to $I = 1$, for chosen bandwidths, both for the single- and many-particle distributions, cf. Figs. 3, 5. This is another indication of strong single- and many-particle localization for the sequence (4).

VII. CONCLUSIONS

In this paper we have explored two aspects of the problem of many-particle localization. One is localization of stationary states. For one-particle states, it has been studied analytically. We found that the wave functions decay quasi-exponentially and obtained the bounds on the decay length. For many-particle states, the decay has been analyzed numerically. Such analysis is unavoidably limited to small chains. For a 12-site chain we have found that, for the on-site energy sequence (18) with the ratio of the single-site energy bandwidth to the hopping integral ≈ 26 [$h/J = 20, \alpha = 0.23, \beta = 0.11$ in Eq. (18)], the inverse participation ratio differs from its value for the case of fully localized states by less than 2%. This deviation is due to a small nonresonant admixture of the wave functions of neighboring sites.

A different approach is based on studying the lifetime of strongly localized states. It is sufficient to have a localization lifetime t_{loc} that exceeds the coherence time of the excitations. We have demonstrated that corresponding t_{loc} can be achieved in a chain of an arbitrary length and with an arbitrary number of excitations. In the explicit construction of on-site energies (18), resonant transitions that lead to delocalization require at least 6 virtual nonresonant steps. This leads to the ratio of the delocalization rate to the intersite hopping integral $\sim 10^{-6}$ already for the geometric-mean amplitude of virtual transitions ~ 0.1 .

An advantageous feature of the sequence (4) and its modification (18) is that one radiation frequency can be used to resonantly excite different qubits. This can be achieved by selectively tuning them to this frequency without bringing neighboring qubits in resonance with each other, or by sweeping the frequency of the targeted qubit through the radiation frequency and having a Landau-Zener-type interstate transition. A two-qubit gate can be conveniently done by selectively tuning neighboring qubits in resonance with each other and having a Landau-Zener type excitation swap [13]. In many cases localization is also a prerequisite for a projective measurement. This happens when the measured quantity is the probability for each qubit to be in the excited state, and a measurement is slow compared to the time J^{-1} of resonant hopping to a nearest site.

For the energy sequence (18) the width of the energy distribution is orders of magnitude smaller than the width that would give the same t_{loc} in the approach to quantum computing with perpetually coupled qubits developed by Benjamin and Bose [11]. In Ref. 11 next nearest neighbors are proposed to be tuned in resonance. Then the localization lifetime is $\sim h/J^2$, where h is the energy difference between nearest neighbors. This difference must exceed J by a factor $\sim 10^5 - 10^6$ in order to have the same localization lifetime as in our approach. Compared to Ref. [10], a potential advantage of our approach is that the interaction does not have to be ever turned off, and no multi-qubit encoding is necessary for

operating a QC.

The presented scheme can be extended to systems with long-range coupling, which also distinguishes it from the approaches [10, 11] that substantially rely on nearest neighbor coupling. For several proposed QC's the interqubit coupling is dipolar for a few near neighbors and becomes quadrupolar or falls down even faster for remote neighbors [2, 3, 4, 6]. Long-range interaction makes transitions over several sites more probable. We leave detailed analysis for a separate paper. Here we only note that, for the sequence (18), not only direct hopping over 2 or 4 sites is not resonant and does not lead to delocalization, but even hopping over 6, 8, or 10 sites is safe in this respect. For all these site separations, the energy difference between the sites is $\sim \alpha h$ or $\sim \beta h/2$, it largely exceeds $2J\Delta$ [for sites separated by an odd number of positions, the energy difference is always large, $\sim h$].

In this paper we have not addressed the question of optimizing the energy sequence, so that maximal localization lifetime could be obtained for a minimal bandwidth of on-site energies. We just demonstrated that one can construct a sequence with a limited bandwidth that gives a long lifetime even for an infinite chain. For a finite-length chain the energy bandwidth can be further reduced using Eq. (4) as an initial approximation and adjusting energies of several specific sites.

In conclusion, we have proposed a sequence of on-site energies (4) and its modification (18) that result in strong localization of all single- and many-particle states in an array of interacting qubits or spins. The sequence (4) has low symmetry, which allows eliminating resonances between the states to a high order in the hopping integral. This leads to strong localization of stationary states in up to a 12 site long chain, as evidenced by numerical calculations. This also leads to a long lifetime of localized many-particle states. The lifetime exceeds the reciprocal hopping integral by 6 orders of magnitude in a chain of arbitrary length provided the bandwidth of on-site energies is larger than the intersite hopping integral by a comparatively small factor of $\sim 25 - 30$. The proposed energy sequence is stable with respect to errors. The results make a scalable quantum computer with perpetually coupled qubits viable, since excitations do not delocalize between gate operations.

Acknowledgments

We are grateful to D.A. Lidar and L.P. Pryadko for the discussion of operation of a quantum computer with perpetually coupled qubits. This work was partly supported by the Institute for Quantum Sciences at Michigan State University and by the NSF through grant No. ITR-0085922.

APPENDIX A: EXPONENTIAL DECAY OF THE TRANSITION AMPLITUDE

In this Appendix we give a rigorous proof of the quasi-exponential decay of the transition amplitude $K_n(m)$ (5) and establish bounds on the exponent. We show that, for the sequence (4), in the limit of small α and for $m \rightarrow \infty$

$$\alpha^{-\nu_L m} \leq K_n(m)(2h/J)^m \leq \alpha^{-\nu_U m}. \quad (\text{A1})$$

We find that $\nu_L \geq 0.89$ and $\nu_U \leq 1.19$.

In order to simplify notations we introduce dimensionless energies $\varepsilon_n(\alpha) = 2\varepsilon_n/h$. From Eq. (4)

$$\varepsilon_n(\alpha) = (-1)^n - \sum_{k=2}^{n+1} (-1)^{\lfloor n/k \rfloor} \alpha^{k-1}. \quad (\text{A2})$$

We also set $J/2h = 1$. Then $K_n(m) = 1/|Q_n(m)|$, where

$$Q_n(m) = \prod_{s=1}^m [\varepsilon_{n+s}(\alpha) - \varepsilon_n(\alpha)]. \quad (\text{A3})$$

From Eq. (A2), $Q_n(m)$ is a polynomial in α .

For a polynomial $P(\alpha)$ we define by $\text{lowdeg } P(\alpha)$ the multiplicity of the root $\alpha = 0$, i.e., the lowest power of α in the polynomial. The exponent ν that characterizes the decay of $K_n(m)$ (6) is given by $\nu = \text{lowdeg } Q_n(m)/m$ for $m \rightarrow \infty$.

The data of the numerical experiments presented in Fig. 2 show that $0.894 < \text{lowdeg } Q_n(m)/m < 1.12$ independent of n for large m .

To obtain an analytical estimate we rewrite Eq. (A3) as

$$\text{lowdeg } Q_n(m) = \sum_{s=1}^m \text{lowdeg}[\varepsilon_{n+s}(\alpha) - \varepsilon_n(\alpha)]. \quad (\text{A4})$$

Each term $\text{lowdeg}[\varepsilon_{n+s}(\alpha) - \varepsilon_n(\alpha)]$ is an integer between 0 and $n+1$.

In order to find bounds for $\text{lowdeg } Q_n(m)$ we will estimate how many terms $\text{lowdeg}[\varepsilon_{n+s}(\alpha) - \varepsilon_n(\alpha)]$ exceed a given i , $0 \leq i \leq n+1$. For each i we have a subset $S_{nm}(i)$ of the values s that satisfy this condition,

$$S_{nm}(i) = \{s \mid 1 \leq s \leq m, \text{lowdeg}[\varepsilon_{n+s}(\alpha) - \varepsilon_n(\alpha)] > i\}. \quad (\text{A5})$$

The number of elements in $S_{nm}(i)$ is denoted by $h_{nm}(i)$. This is the number of polynomials $\varepsilon_{n+s}(\alpha) - \varepsilon_n(\alpha)$ whose expansion in α starts with α^k with $k > i$. In what follows for brevity we drop the subscripts n, m and use $S(i)$ and $h(i)$ for $S_{nm}(i)$ and $h_{nm}(i)$.

It follows from the definition that

$$h(0) \geq h(1) \geq h(2) \geq \dots \geq h(n).$$

By construction

$$\begin{aligned} \text{lowdeg } Q_n(m) &= \sum_{i=1}^n i[h(i-1) - h(i)] \\ &\quad + (n+1)h(n) = \sum_{i=0}^n h(i) \end{aligned} \quad (\text{A6})$$

From Eq. (A6) we see that the upper and lower bounds on $\text{lowdeg } Q_n(m)$ are given by the sums of the upper and lower bounds of $h(i)$.

In what follows we will use the standard notations: \liminf (\limsup) means the lower (upper) limit of a sequence, $\text{LCM}\{i_1, \dots, i_r\}$ is the least common multiple of integers i_1, \dots, i_r , and $\text{GCD}\{i_1, \dots, i_r\}$ is the greatest common divisor of i_1, \dots, i_r . We will also denote by $[\varepsilon(\alpha)]_k$ the coefficient at α^k in the polynomial $\varepsilon(\alpha)$, i.e.,

$$\varepsilon_n(\alpha) = \sum_{k=0}^n [\varepsilon_n(\alpha)]_k \alpha^k. \quad (\text{A7})$$

1. Lower bound

In this section we obtain the lower bound of $\text{lowdeg } Q_n(m)$. The main statement is the following lemma.

Lemma A.1 *The lower bound has the form*

$$\liminf_{m \rightarrow \infty} \frac{\text{lowdeg } Q_n(m)}{m} \geq 0.89.$$

Proof. Consider first the constant term $[\varepsilon_n(\alpha)]_0$ in Eq. (A7). By definition, $[\varepsilon_n(\alpha)]_0 = [\varepsilon_{n+2}(\alpha)]_0$, and

$$\text{lowdeg}(\varepsilon_{n+s}(\alpha) - \varepsilon_n(\alpha)) = \begin{cases} 0 & \text{for odd } s, \\ \geq 1 & \text{for even } s. \end{cases}$$

Hence, we immediately obtain a simple lower bound $\text{lowdeg } Q_n(m) \geq \lfloor m/2 \rfloor$ for large m (in what follows we always imply $m \rightarrow \infty$).

We compute $h(0)$, $h(1)$, etc, using that the coefficients $[\varepsilon_n(\alpha)]_i$ are periodic in n with period $2(i+1)$. Indeed, from Eq. (A2),

$$\begin{aligned} [\varepsilon_n(\alpha)]_i &= (-1)^{\lfloor n/(i+1) \rfloor} \\ &= (-1)^{\lfloor [n+2(i+1)]/(i+1) \rfloor} = [\varepsilon_{n+2(i+1)}(\alpha)]_i. \end{aligned}$$

Therefore, the sets of coefficients $\{[\varepsilon_n(\alpha)]_0, [\varepsilon_n(\alpha)]_1, \dots, [\varepsilon_n(\alpha)]_i\}$ are also periodic in n , but with the period $T_i = 2 \text{LCM}\{2, 3, \dots, i+1\}$. This is illustrated by the table

$$\begin{aligned} \varepsilon_1(\alpha) &= -1 \quad -\alpha \\ \varepsilon_2(\alpha) &= 1 \quad +\alpha \quad -\alpha^2 \\ \varepsilon_3(\alpha) &= -1 \quad +\alpha \quad +\alpha^2 \quad -\alpha^3 \\ \varepsilon_4(\alpha) &= 1 \quad -\alpha \quad +\alpha^2 \quad +\alpha^3 \quad -\alpha^4 \\ \varepsilon_5(\alpha) &= -1 \quad -\alpha \quad +\alpha^2 \quad +\alpha^3 \quad +\alpha^4 \quad -\alpha^5 \\ \varepsilon_6(\alpha) &= 1 \quad +\alpha \quad -\alpha^2 \quad +\alpha^3 \quad +\alpha^4 \quad +\alpha^5 \quad -\alpha^6 \\ \varepsilon_7(\alpha) &= -1 \quad +\alpha \quad -\alpha^2 \quad +\alpha^3 \quad +\alpha^4 \quad +\alpha^5 \quad +\alpha^6 \quad -\alpha^7 \end{aligned}$$

In order to estimate $h(i)$ we need two technical statements.

Lemma A.2 Let a_0, k, T be any integers such that $2k$ does not divide T . Consider any $2k/\text{GCD}\{T, 2k\}$ consecutive elements of an arithmetic progression $a_j = a_0 + j \cdot T$, and set $b_j = \lfloor a_j/k \rfloor \bmod 2$.

Then, at least $\lfloor k/\text{GCD}\{T, 2k\} \rfloor$ integers b_j are equal to 0, and at least the same number of b_j are equal to 1.

Proof. Since $2k$ does not divide T , the sequence $a_j \bmod 2k$ is cyclic in the interval $[0, 2k-1]$. This sequence contains exactly $2k/\text{GCD}\{T, 2k\}$ distinct elements. On average, half of them (at least $\lfloor p/\text{GCD}\{T, 2k\} \rfloor$) are less than p , and another half (the same number) are larger or equal than p . This means that there are at least $\lfloor k/\text{GCD}\{T, 2k\} \rfloor$ integers b_j that are equal to 0 and at least the same number of b_j that are equal to 1. Q.E.D.

The next statement is a corollary of lemma A.2 and we skip the proof.

Corollary A.3 Let $2k$ does not divide T . Consider p consecutive elements of the arithmetic progression $a_j = a_0 + j \cdot T$ and set $b_j = \lfloor a_j/k \rfloor \bmod 2$.

Then at least $\lfloor k/\text{GCD}\{T, 2k\} \rfloor \lfloor p \cdot \text{GCD}\{T, 2k\}/2k \rfloor$ integers b_j are equal to 0, and at least the same number of b_j are equal to 1.

We are now in a position to finish the proof of Lemma A.1. We notice first that, for $n = a_j$ in the expression (A2), the coefficient b_j for given k determines the sign of the term α^{k-1} in $\varepsilon_n(\alpha)$, that is $(-1)^{b_j} = [\varepsilon_n(\alpha)]_{k-1}$. The number $h(i)$ gives the probability that, for all $k \leq i$, the polynomial $\varepsilon_{n+s}(\alpha)$ has the same b_j as $\varepsilon_n(\alpha)$.

We will now estimate $h(i)$ with $i = 1, \dots, 4$ and start with $h(1)$. We note that $s \in S(1)$ if and only if $s \in S(0)$ and $[\varepsilon_{n+s}]_1 = [\varepsilon_n]_1$. The second condition means that $\lfloor s/2 \rfloor \bmod 2 = 0$. By construction (A5), for $m \rightarrow \infty$ the set $S(0)$ is formed by all numbers s of the same parity as n . This means that $S(0)$ is an arithmetic progression with period $T_0 = 2$. We take p consecutive elements s_1, \dots, s_p of it and use Corollary A.3 with $k = 2$, because we are interested in the coefficients $[\varepsilon_{n+s_i}]_1 = (-1)^{\lfloor (n+s_i)/2 \rfloor}$ in (A2). By Corollary A.3, since T_0 is not divisible by $2k$, for at least $\lfloor p/2 \rfloor$ subscripts s_i the coefficients $[\varepsilon_{n+s_i}(\alpha)]_1 = 1$, and $[\varepsilon_{n+s_i}(\alpha)]_1 = -1$ for at least the same amount of subscripts s_i , i.e., approximately half of the coefficients $[\varepsilon_{n+s_i}(\alpha)]_1$ coincide with $[\varepsilon_n(\alpha)]_1$. Hence, $h(1) \geq h(0)/2$ as $m \rightarrow \infty$. Substituting $h(0) = m/2$ we obtain $h(1) = m/4$.

Similar arguments can be applied to estimate $h(2)$. This requires finding a portion of the set $S(1)$ which forms $S(2)$. The set $S(1)$ is a nonempty disjoint union of arithmetic progressions with period $T_1 = 4$. We will apply Corollary A.3 with $k = 3$ to each of these progressions and use $p = h(1)$. This gives $h(2) \geq \lfloor 3/2 \rfloor \lfloor (1/3)(m/4) \rfloor = \lfloor m/12 \rfloor$, or $h(2)/m \geq 1/12$ for $m \rightarrow \infty$.

In the same way we obtain $h(3)/m \geq 1/24$ and $h(4)/m \geq 1/60$ as $m \rightarrow \infty$. Therefore

$$\text{lowdeg } Q_n(m)/m \geq \frac{1}{2} + \frac{1}{4} + \frac{1}{12} + \frac{1}{24} + \frac{1}{60} \geq 0.89,$$

which finishes the proof of the lower bound.

2. Upper bound

We start with the proof of the following rough estimate:

Lemma A.4 An upper bound has the form

$$\limsup_{n \rightarrow \infty} \frac{\text{lowdeg } Q_n(m)}{m} \leq \frac{22}{15} < 1.47.$$

Proof. Taking in the rhs of Eq. (A6) the sum from 0 to ∞ we obtain

$$\text{lowdeg } Q_n(m) \leq \sum_{i=0}^{\infty} h(i). \quad (\text{A8})$$

To find an upper bound on $h(i)$ we will use the following consequence of Lemma A.2:

Corollary A.5 Let $2k$ does not divide T . Consider p consecutive elements of the arithmetic progression $a_j = a_0 + j \cdot T$ and set $b_j = \lfloor a_j/k \rfloor \bmod 2$.

Then at most

$$\left(\frac{2k}{\text{GCD}\{T, 2k\}} - \left\lfloor \frac{k}{\text{GCD}\{T, 2k\}} \right\rfloor \right) \times \left(\left\lfloor \frac{p \cdot \text{GCD}\{T, 2k\}}{2k} \right\rfloor + 1 \right)$$

integers b_j are equal to 0, and at most the same number of b_j are equal to 1.

Using the same arguments as before, by corollary A.5 we obtain for $m \rightarrow \infty$ the following upper bounds for $h(i)$

$$\begin{aligned} h(0) &\leq m/2, \\ h(1) &\leq m/4, \\ h(2) &\leq m/6, \\ h(3) &\leq m/12, \\ h(4) &\leq m/20. \end{aligned} \quad (\text{A9})$$

Recall that $h(4) \geq h(5) \geq h(6) \geq h(7)$. Similarly, for $q \geq 2$ we have

$$h(2^q) \geq h(2^q + 1) \geq \dots h(2^{q+1} - 1).$$

Therefore we can replace the terms $h(2^q + 1), \dots, h(2^{q+1} - 1)$ in the rhs of Eq. (A8) by

$h(2^q)$, which leads to the following upper bound for $\text{lowdeg } Q_n(m)$,

$$\text{lowdeg } Q_n(m) \leq h(0) + h(1) + h(2) + h(3) + \sum_{q=2}^{\infty} 2^q h(2^q). \quad (\text{A10})$$

This reduces the calculation to finding upper bounds on $h(2^q)$.

We will now obtain a recurrence relation for $h(2^q)$. First we notice that, for $K+1$ being a prime number, we have from Corollary A.5

$$h(K+1) \leq \frac{K+2}{2(K+1)} h(K). \quad (\text{A11})$$

For all primes $K+1 \geq 7$ we have $(K+2)/2(K+1) \leq 4/7$. Therefore $h(K+1) \leq \frac{4}{7}h(K)$ for $K \geq 6$. We also note that, for all positive integral q ,

$$h(2^q) \leq \frac{1}{2}h(2^q - 1).$$

Now we recall the distribution law for primes in the intervals. The following statement is called Bertrand's

postulate (or Tchebychev' theorem) (see Ref. 16):

Theorem A.6 *There is at least one prime between M and $2M$ for any positive integer M . If $M > 3$, there is always at least one prime between M and $2M - 2$.*

In particular, there is at least one prime between 2^q and $2^{q+1} - 1$ for any positive integer $q \geq 2$. With this statement, taking into account the previous estimates, we obtain

$$h(2^{q+2}) \leq \left(\frac{1}{2} \cdot \frac{4}{7}\right)^q \frac{m}{20}$$

for all positive integral q , or

$$h(2^{q+2}) \leq \left(\frac{2}{7}\right)^q \frac{m}{20}. \quad (\text{A12})$$

Substituting inequalities (A9), (A12) into (A10), we obtain

$$\begin{aligned} \text{lowdeg } Q_n(m) &\leq \frac{m}{2} + \frac{m}{4} + \frac{m}{6} + \frac{m}{12} + \frac{m}{20} \left(2^2 + 2^3 \cdot \frac{2}{7} + 2^4 \left(\frac{2}{7}\right)^2 + \dots + 2^k \left(\frac{2}{7}\right)^{k-2} + \dots \right) \\ &= m \left(1 + \frac{2^2}{20} \sum_{j=0}^{\infty} \left(\frac{4}{7}\right)^j \right) \quad \text{for } m \rightarrow \infty. \end{aligned}$$

This gives

$$\text{lowdeg } Q_n(m) \leq \frac{22}{15}m < 1.47m \quad (\text{A13})$$

The last inequality is an explicit asymptotic upper bound. Q.E.D.

We now provide a sharper upper bound. We will use the same method, but instead of Tchebyshev' theorem we will apply Erdős theorem.

Lemma A.7 *(Sharper bound)*

$$\limsup_{m \rightarrow \infty} \frac{\text{lowdeg } Q_n(m)}{m} \leq 1.19$$

Proof. Following the same pattern as in Lemma A.4 above we extend the explicit list of inequalities (A9).

As $m \rightarrow \infty$,

$$\begin{aligned} h(5)/m &\leq 1/20, \\ h(6)/m &\leq 1/35, \\ h(7)/m &\leq 1/70, \\ h(8)/m &\leq 1/126, \\ h(9)/m &\leq 1/126, \\ h(10)/m &\leq 1/231, \\ h(11)/m &\leq 1/231, \\ h(12)/m &\leq 1/429, \\ h(13)/m &\leq 1/429, \\ h(14)/m &\leq 1/429, \\ h(15)/m &\leq 1/858, \\ h(16)/m &\leq 3/4862. \end{aligned} \quad (\text{A14})$$

To obtain a sharper upper bound we recall the following result by Erdős [17].

Theorem A.8 (Erdős) *There exist at least one prime of the form $4k+1$ and at least one prime of the form $4k+3$*

between M and $2M$ for all $m > 6$.

For all primes that exceed 16 we have in Eq. (A11) $(K+2)/2(K+1) < 7/13$. Therefore, by reproducing the arguments that led to the inequality (A12), but using now the relation (A11) twice based on the theorem A.8, we obtain

$$h(2^{q+4}) \leq \left[\frac{1}{2} \cdot \left(\frac{7}{13} \right)^2 \right]^q h(16). \quad (\text{A15})$$

Substituting inequalities (A9), (A14), (A15) into (A10) (where now the terms up to $h(15)$ are taken into account explicitly, and the sum runs from $q = 4$) we obtain

$$\begin{aligned} \limsup_{m \rightarrow \infty} \frac{\text{lowdeg } Q_{n,m}}{m} &\leq \frac{1}{2} + \frac{1}{4} + \frac{1}{6} + \frac{1}{12} + \frac{2}{20} \\ &+ \frac{1}{35} + \frac{1}{70} + \frac{2}{126} + \frac{2}{231} + \frac{3}{429} + \frac{1}{858} \\ &+ \frac{3 \cdot 16}{4862} \left(1 + \left(\frac{7}{13} \right)^2 + \left(\frac{7}{13} \right)^4 + \dots \right). \end{aligned}$$

Evaluating the rhs, we obtain

$$\limsup_{m \rightarrow \infty} \frac{\text{lowdeg } Q_n(m)}{m} < 1.19. \quad (\text{A16})$$

Q.E.D.

[1] M. A. Nielsen and I. L. Chuang, *Quantum Computation and Quantum Information* (Cambridge University Press, Cambridge, 2000).

[2] Y. Makhlin, G. Schön, and A. Shnirman, Rev. Mod. Phys. **73**, 357 (2001).

[3] P. M. Platzman and M. I. Dykman, Science **284**, 1967 (1999).

[4] J. E. Mooij, T. P. Orlando, L. Levitov, L. Tian, C. H. van der Wal, and S. Lloyd, Science **285**, 1036 (1999).

[5] T. D. Ladd, J. R. Goldman, F. Yamaguchi, Y. Yamamoto, E. Abe, and K. M. Itoh, Phys. Rev. Lett. **89**, 017901 (2002).

[6] Yu. A. Pashkin, T. Yamamoto, O. Astafiev, Y. Nakamura, D. V. Averin, and J. S. Tsai, Nature **421**, 823 (2003).

[7] W. G. Van der Wiel, S. De Franceschi, J. M. Elzerman, T. Fujisawa, S. Tarucha, and L. P. Kouwenhoven, Rev. Mod. Phys. **75**, 1 (2003).

[8] E. Abrahams, S.V. Kravchenko, and M.P. Sarachik, Rev. Mod. Phys. **73**, 251 (2001).

[9] B. Georgeot and D. L. Shepelyansky, Phys. Rev. E **62**, 3504, 6366 (2000).

[10] X. Zhou, Z. Zhou, G. Guo, and M. J. Feldman, Phys. Rev. Lett. **89**, 197903 (2002).

[11] S. C. Benjamin and S. Bose, Phys. Rev. Lett. **90**, 247901 (2003).

[12] G. P. Berman, F. Borgonovi, F. M. Izrailev, and V. I. Tsifrinovich, Phys. Rev. E **64**, 056226 (2001); **65**, 015204 (2002).

[13] M. I. Dykman and P. M. Platzman, Fortschr. Phys. **48**, 9 (2000); Quantum Inf. Comput. **1**, 102 (2001).

[14] P. Jordan and E. Wigner, Z. Phys. **47**, 631 (1928).

[15] P. W. Anderson, Phys. Rev. **109**, 1492 (1958).

[16] T. Nagell, *Introduction to Number Theory* (Wiley, New York 1951).

[17] P. Erdős, J. London Math. Soc. **9**, 282 (1934).